POLISH JOURNAL *of* RADIOLOGY

Original paper

Computed tomography radiomics combined with clinical parameters for hepatocellular carcinoma differentiation: a machine learning investigation

Shijing Ma[1,2], Yingying Zhu[3], Changhong Pu[2], Jin Li[1,4], Bin Zhong[1,5]

[1]School of Basic Medical Sciences, Youjiang Medical University for Nationalities, Baise City, China
[2]Department of Radiology, Affiliated Hospital of Youjiang Medical University for Nationalities, Baise City, China
[3]Baise City People's Hospital, Baise City, China
[4]Department of Biochemistry, Faculty of Medicine, Chiang Mai University, Chiang Mai, Thailand
[5]Modern Industrial College of Biomedicine and Great Health, Youjiang Medical University for Nationalities, Baise City, China

Abstract

Purpose: To evaluate the performance of a combined clinical-radiomics model using multiple machine learning approaches for predicting pathological differentiation in hepatocellular carcinoma (HCC).

Material and methods: A total of 196 patients with pathologically confirmed HCC, who underwent preoperative computed tomography (CT) were retrospectively enrolled (training: $n = 156$; validation: $n = 40$). The modelling process included the following: (1) clinical model construction through logistic regression analysis of risk factors; (2) radiomics model development by comparing 6 machine learning classifiers; and (3) integration of optimal clinical and radiomic features into a combined model. Model performance was assessed using the area under the curve (AUC), calibration curves, and decision curve analysis (DCA). A nomogram was constructed for clinical implementation.

Results: Two clinical risk factors (BMI and CA153) were identified as independent predictors of differentiated HCC. The clinical model showed moderate performance (AUC: training = 0.705, validation = 0.658). The radiomics model demonstrated improved prediction capability (AUC: training = 0.840, validation = 0.716). The combined model achieved the best performance in differentiating HCC pathological grades (AUC: training = 0.878, validation = 0.747).

Conclusions: The integration of CT radiomics features with clinical parameters through machine learning provides a promising non-invasive approach for predicting HCC pathological differentiation. This combined model could serve as a valuable tool for preoperative treatment planning.

Key words: hepatocellular carcinoma, computed tomography, radiomics, machine learning, pathological grading.

Introduction

The incidence of hepatocellular carcinoma (HCC), the predominant form of primary liver cancer, continues to rise globally, making it a significant cause of cancer-related mortality [1,2]. Accurate preoperative assessment of HCC pathological differentiation is crucial because it directly influences treatment planning and patient outcomes [3,4]. Evidence suggests that patients with well to moderately differentiated HCC demonstrate superior overall survival rates and lower recurrence risks compared to those with poorly differentiated tumours [5,6].

Although postoperative pathological examination remains the gold standard for determining HCC differentia-

tion, its invasive nature and potential sampling bias limitations necessitate the development of reliable non-invasive alternatives [7,8]. Conventional imaging approaches using computed tomography (CT), magnetic resonance imaging (MRI), and ultrasound have shown limited success in predicting HCC differentiation grades, primarily due to their dependence on subjective radiological interpretation and restricted feature analysis [9-13].

Radiomics, an emerging field that transforms medical images into high-dimensional quantitative data, has demonstrated promising results in tumour characterisation [14,15]. Recent studies have successfully applied radiomics analysis in various aspects of HCC management, including biomarker prediction, recurrence assessment, and survival prognosis [16-18]. However, research specifically focusing on radiomics-based prediction of HCC pathological differentiation remains limited, with unresolved questions regarding optimal classifier selection and model generalisability [19-21].

The present study aims to develop and validate a combined clinical-radiomics model for preoperative prediction of HCC pathological differentiation. By integrating clinical parameters with radiomics features and presenting the results through a practical nomogram, we seek to establish a more accurate and clinically applicable tool for personalised HCC treatment planning.

Material and methods

Ethical considerations

The institutional Ethics Committee of Youjiang Medical University for Nationalities approved this retrospective investigation (approval number: 2018010401) and waived the requirement for informed consent due to the study design. All procedures were performed in accordance with relevant guidelines and regulations.

Patients

A total of 242 patients with HCC who underwent preoperative CT examination between January 2018 and June 2023 were initially considered for this study. The inclusion criteria were as follows: (1) histopathologically confirmed HCC; (2) availability of abdominal CT scans within 2 weeks before surgery; (3) complete clinical and CT image data; and (4) willingness to provide follow-up information. Patients were excluded if they had: (1) unconfirmed HCC diagnosis; (2) benign or mixed liver tumours; (3) incomplete clinical records; (4) CT images with significant artifacts or unclear lesions; (5) concurrent malignancies in other organs; or (6) lesions that could not be accurately delineated. After applying these criteria, 196 patients were included in the final analysis (Figure 1). For the included patients, clinical information encompassed demographic data, laboratory test results, tumour markers, and detailed surgical/pathological reports. CT examinations were performed with slice thickness ≤ 5 mm, and all images were confirmed to be free from significant artifacts or quality issues that might affect analysis.

CT examination

All CT examinations were performed using a GE Revolution 256-slice CT scanner (Revolution, GE Healthcare, USA). The scanning range covered from the diaphragm to the lower edge of the liver. The scanning parameters were as follows: collimator, 64×0.625 mm; rotation time, 0.80 s; pitch, 0.984;
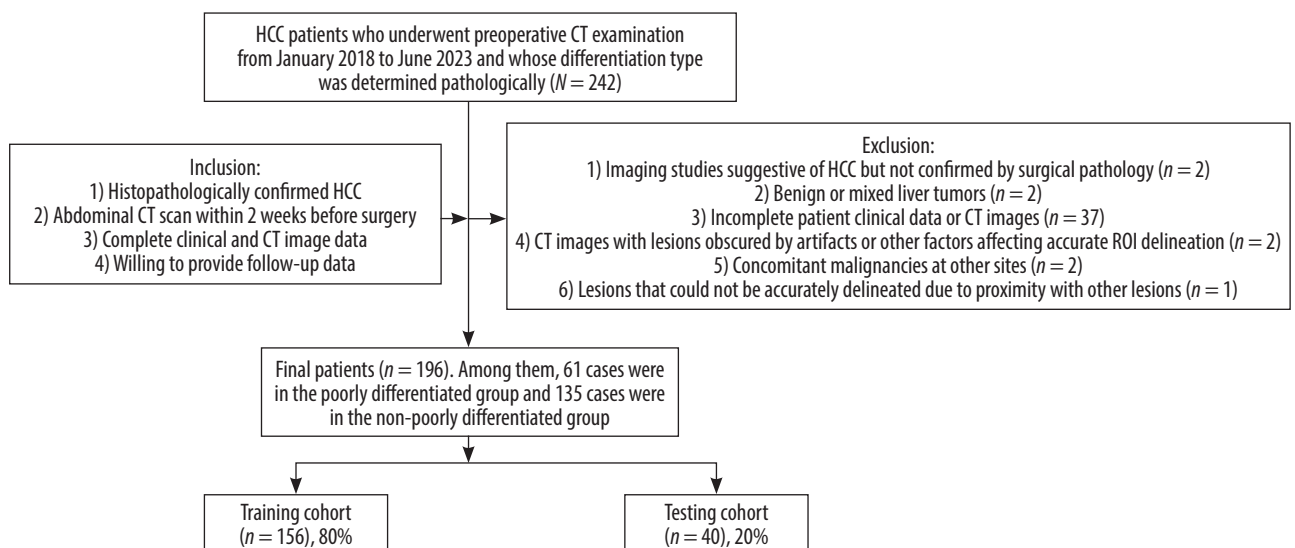

Figure 1. The workflow diagram showing the patient selection process. The study initially identified 242 HCC patients between January 2018 and June 2023. After applying inclusion and exclusion criteria, 196 patients were finally enrolled and divided into training ($n = 156$) and testing ($n = 40$) cohorts

HCC – hepatocellular carcinoma, CT – computed tomography

matrix, 512 × 512; field of view, 350 mm × 350 mm; tube voltage, 120 kV; tube current, 200-420 mAs; and slice thickness and interval, 5 mm.

Patient groups and clinical data

The study cohort was randomly divided into training ($n = 156$, 80%) and validation ($n = 40$, 20%) groups. Clinical data included laboratory parameters (including albumin, alanine aminotransferase (ALT), aspartate aminotransferase (AST), α-fetoprotein (AFP), cancer antigens 153 (CA153), cancer antigens 199 (CA199), carcinoembryonic antigen (CEA), and microvascular invasion (MVI) etc.), demographic information (age, gender), and relevant clinical history (smoking and drinking). HCC differentiation was classified according to World Health Organisation criteria [22], with patients categorised into poorly differentiated and non-poorly differentiated (moderately and well differentiated) groups.

Image preprocessing and segmentation

CT images were preprocessed using Pyradiomics (version 3.7.12) with standardisation to $1 \times 1 \times 1$ mm voxel spacing. Two radiologists (with 12 and 5 years of experience in abdominal imaging) independently performed tumour segmentation on non-enhanced CT images using ITK-SNAP software. Inter-observer agreement was assessed using intraclass correlation coefficients (ICC). Any discrepancies were resolved through consensus or consultation with a senior radiologist.

Radiomics feature extraction

A total of 1834 radiomics features were extracted from each ROI using Pyradiomics (version 3.7.12). Among these features, wavelet-based texture features were computed through a 3-step process. Taking 'wavelet_LHL_glcm_InverseVariance' as an example:
1) the wavelet transformation was applied to decompose the original image:

$$W(a,b) = (1/\sqrt{|a|}) \int f(t) \, \mathbb{O} \, \psi((t-b)/a)dt$$

where the LHL sub-band represents high-frequency components in the x and z directions and low-frequency components in the y direction;
2) the Gray-Level Co-occurrence Matrix (GLCM) P(i,j) was computed from the wavelet sub-band:

$$P(i,j) = N(i,j) / \Sigma\Sigma N(i,j)$$

where $N(i,j)$ represents the frequency of occurrence of pixel pairs with values i and j;
3) the inverse variance was calculated as:

$$\text{Inverse variance} = \Sigma\Sigma P(i,j) / (1 + (i-j)^2)$$

where i and j are the row and column indices in the GLCM, quantifying local homogeneity of the texture.

These features included the following: first-order statistics, shape-based features, and texture features derived from Grey Level Co-occurrence Matrix (GLCM), Grey Level Correlation Matrix (GLDM), Grey Level Run Length Matrix (GLRLM), Gray Level Size Zone Matrix (GLSZM), and Neighbourhood Grey Level Tone Difference Matrix (NGTDM).

Feature selection and radiomics score calculation

The radiomics features underwent sequential processing: (1) normalisation through regularisation; (2) Spearman correlation analysis with correlation threshold of 0.9; (3) Mann-Whitney test with $p < 0.05$ significance level; and (4) LASSO regression with 10-fold cross-validation for feature selection. The optimal lambda value in LASSO regression was determined through 10-fold cross-validation, mathematically expressed as:

$$\lambda\_optimal = argmin\_\lambda \{(1/10) \textstyle\sum_i MSE\_i(\lambda)\}$$

where $MSE\_i(\lambda)$ represents the mean squared error for the i-th fold validation set using regularisation parameter λ. This process involved the following: 1) dividing the dataset into 10 equal-sized subsets; 2) training the model on 9 subsets and validating on the remaining subset; 3) computing MSE for each validation; 4) averaging MSE across all 10 folds; and 5) selecting the lambda value that minimised the average MSE.

The final radiomics score was calculated using the formula: Rad score = $\beta0 + \beta1X1 + \beta2X2 + ... + \beta nXn$, where βn represents the coefficient and Xn represents the selected feature. The workflow is illustrated in Figure 2.

Model development

Clinical variables were analysed using univariate and multivariate logistic regression to identify independent predictors of HCC differentiation ($p < 0.05$). The selection of machine learning classifiers was based on computational efficiency and clinical interpretability considerations. Given our dataset size ($n = 196$) and available computational resources, we prioritised models that provided optimal performance while maintaining interpretability. Advanced ensemble methods such as XGBoost and Random Forest were not included due to their high computational overhead and reduced interpretability in clinical settings. For the radiomics model, 6 machine learning classifiers were evaluated: logistic regression, support vector machine, K-nearest neighbour, extra trees, light gradient boosting machine, and multilayer perceptron. The best-performing classifier was selected based on the area under the receiver operating characteristic curve (AUC) in the validation set. Five-fold cross-validation was performed to ensure model robustness.
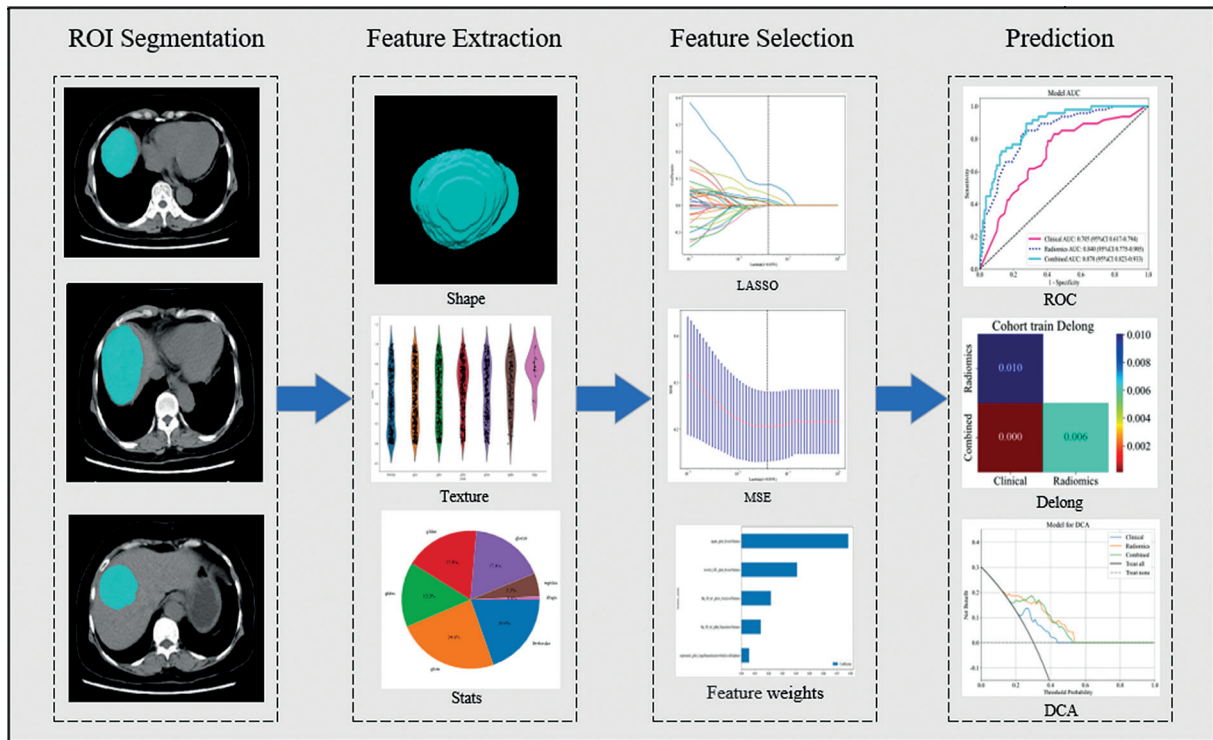
Figure 2. Radiomics workflow showing the process of ROI segmentation, feature extraction, feature selection, and prediction model development

Abbreviations: ROC – receiver operating characteristic, DCA – decision curve analysis

A combined model was then constructed by integrating the optimal radiomics model with significant clinical predictors. Model performance was assessed through receiver operating characteristic (ROC) curve analysis, and the DeLong test was used to compare AUCs between different models. A nomogram was developed to facilitate clinical implementation of the combined model. Decision curve analysis (DCA) was performed to evaluate the clinical utility of each model.

Statistical analysis

Continuous variables were compared using Student's *t*-test or the Mann-Whitney *U* test based on their distribution (assessed by the Shapiro-Wilk test), while categorical variables were analysed using the χ^2 test. Clinical characteristics analysed included BMI, CA153, CA199, prothrombin, gender, smoking status, alcohol consumption, hepatitis history, age, albumin, ALT, AST, AFP, CEA, and MVI status.

Feature selection involved multiple steps: (1) correlation analysis using Spearman coefficients (threshold > 0.9 for removal); (2) recursive feature elimination; and (3) LASSO regression for final feature selection. Model performance metrics included sensitivity, specificity, accuracy, and AUC. All statistical analyses were performed using Python (version 3.7.12), with $p < 0.05$ considered statistically significant.

Results

Patient characteristics

The study included 196 patients with histologically confirmed HCC, divided into training ($n = 156$) and testing ($n = 40$) cohorts. Baseline characteristics of both cohorts are presented in Table 1. The mean age was 50.54 ± 11.58 years in the training cohort and 52.52 ± 10.94 years in the testing cohort. Most patients were male (84.71% in the training cohort and 80.00% in the testing cohort). In both cohorts, most patients had hepatitis (80.77% and 72.50%, respectively) and normal albumin levels (74.36% and 77.50%, respectively). Between the training and testing cohorts, significant differences were observed in BMI (22.49 ± 3.48 vs. 21.92 ± 3.14 kg/m², $p = 0.006$) and MVI status (37.82% vs. 40.00%, $p = 0.049$). Other clinical parameters, including tumour markers (CA153, CA199, AFP, CEA), liver function tests (ALT, AST), and demographic characteristics showed no significant differences between the cohorts (all $p > 0.05$).

Univariate and multivariate logistic analysis and construction of clinical models

Univariate and multivariate logistic analyses were performed to identify predictive factors for the pathological differentiation in HCC patients. Univariate analysis

identified 13 variables significantly associated with HCC differentiation ($p < 0.05$), including sex, smoking status, drinking status, hepatitis, age, albumin, ALT, AST, AFP, BMI, prothrombin, MVI, and CA153 (Table 2). In the subsequent multivariate analysis, only BMI (OR: 0.923, 95% CI: 0.875-0.973, $p = 0.013$) and CA153 (OR: 1.061, 95% CI: 1.020-1.102, $p = 0.012$) remained as independent predictors. The clinical model achieved AUCs of 0.705 (95% CI: 0.617-0.794) in the training cohort and 0.658 (95% CI: 0.472-0.844) in the testing cohort (as shown in Figure 4C and D).

Radiomic feature selection and radiomics score

A total of 1834 radiomic features were extracted from tumour ROIs on preoperative CT images, encompassing first-order statistics, shape-based features, and texture parameters (GLDM, GLRLM, GLSZM, and NGTDM).

The LASSO regression analysis was performed for feature selection and dimensionality reduction (Figure 3). The coefficient paths of different features are shown in Figure 3A, where the vertical dashed line indicates the optimal lambda value ($\lambda = 0.0391$). Figure 3B demonstrates the mean squared error at varying lambda values during 10-fold cross-validation. At the optimal lambda, 5 non-zero coefficient features were selected from the training cohort. The relative importance and coefficient values of these selected features are presented in Figure 3C.

The radiomics score was calculated using the following formula:

Rad_score = 0.30128205128205127

+0.005545 · exponential_gldm_LargeDependence-LowGrayLevelEmphasis

+0.021482 · lbp_3D_m1_glszm_GrayLevelVariance

+0.014065 · lbp_3D_m2_gldm_DependenceVariance

+0.078159 · square_glcm_InverseVariance

+0.040663 · wavelet_LHL_glcm_InverseVariance

Radiomics model establishment and selection

Six machine learning classifiers were evaluated to develope the radiomics model, including logistic regression (LR), support vector machine (SVM), k-nearest neighbours (KNN), extra trees, light gradient boosting machine (LightGBM), and multilayer perceptron (MLP). The ROC curves in Figures 4A-B provide a comprehensive comparison of the discrimination performance of the different radiomics models evaluated in this study. The LightGBM algorithm achieved the highest performance with AUCs of 0.840 (95% CI: 0.775-0.905) in the training cohort and 0.716 (95% CI: 0.537-0.894) in the testing cohort (Figure 4A and B). Based on its superior performance, LightGBM was selected for the construction of the final radiomics model. Therefore, when building the integrated combined model combining clinical features

Table 1. Clinical characteristics of patients in the training and testing cohorts

Feature name	Train-label ($n = 156$)	p-value	Test-label ($n = 40$)	p-value
BMI (kg/m²)	22.49 ± 3.48	0.268	21.92 ± 3.14	0.006*
Prothrombin	12.83 ± 7.56	0.287	11.52 ± 1.86	0.989
Age (years)	50.54 ± 11.58	0.516	52.52 ± 10.94	0.685
CA153	15.03 ± 8.59	0.137	15.12 ± 14.38	0.977
CA199	42.39 ± 101.56	0.753	32.27 ± 62.02	0.876
Sex		0.206		1.0
Female	23 (14.74)		8 (20.00)	
Male	133 (84.71)		32 (80.00)	
Smoke		0.921		0.608
No	97 (62.18)		25 (62.50)	
Yes	59 (37.82)		15 (37.50)	
Drink		1.0		0.219
No	87 (55.77)		28 (70.00)	
Yes	69 (44.23)		12 (30.00)	
Hepatitis		0.496		1.0
No	30 (19.23)		11 (27.50)	
Yes	126 (80.77)		29 (72.50)	
Albumin (g/dl)		1.0		0.781
Normal	116 (74.36)		31 (77.50)	
Abnormal	40 (25.64)		9 (22.50)	
ALT (U/l)		0.993		1.0
< 40	98 (62.82)		28 (70.00)	
≥ 40	58 (37.18)		12 (30.00)	
AST (U/l)		0.577		0.763
< 40	86 (55.13)		23 (57.50)	
≥ 40	70 (44.87)		17 (42.50)	
AFP (ng/mL)		0.257		0.219
< 25	62 (39.74)		21 (52.50)	
≥ 25	94 (60.26)		19 (47.50)	
CEA (ng/ml)		0.562		0.571
< 5	141 (90.38)		37 (92.50)	
≥ 5	15 (9.62)		3 (7.50)	
MVI		0.327		0.049*
No	97 (62.18)		24 (60.00)	
Yes	59 (37.82)		16 (40.00)	

Values are presented as mean ± standard deviation or n (%).
*Indicates statistical significance (p < 0.05).
BMI – body mass index, CA153 – cancer antigen 153, CA199 – cancer antigen 199, ALT – alanine aminotransferase, AST – aspartate aminotransferase, AFP – alpha-fetoprotein, CEA – carcinoembryonic antigen, MVI – microvascular invasio

Table 2. Univariate and multivariate analysis for predicting HCC pathological differentiation

Variable	Univariate analysis OR (95%)	*p*-value	Multivariable analysis OR (95%)	*p*-value
Sex	0.385 (0.280-0.530)	0.001*	0.469 (0.193-1.142)	0.162
Smoke	0.405 (0.252-0.649)	0.002*	0.494 (0.162-1.502)	0.297
Drink	0.437 (0.285-0.673)	0.002*	1.739 (0.602-5.023)	0.391
Hepatitis	0.465 (0.340-0.637)	0.001*	2.213 (0.908-5.398)	0.143
Age	0.455 (0.243-0.851)	0.039*	1.031 (0.462-2.303)	0.950
Albumin	0.429 (0.243-0.756)	0.014*	0.823 (0.391-1.730)	0.666
ALT	0.450 (0.282-0.717)	0.005*	1.669 (0.702-4.112)	0.324
AST	0.373 (0.240-0.580)	0.001*	0.504 (0.215-1.183)	0.186
AFP	0.516 (0.361-0.739)	0.002*	1.405 (1.026-1.328)	0.408
CEA	0.667 (0.280-1.586)	0.442		
BMI	0.963 (0.951-0.975)	0.001*	0.923 (0.875-0.973)	0.013*
Prothrombin	0.940 (0.919-0.962)	0.001*	0.982 (0.939-1.026)	0.500
MVI	0.553 (0.353-0.864)	0.029*	1.645 (0.896-3.111)	0.199
CA153	0.968 (0.952-0.984)	0.001*	1.061(1.020-1.102)	0.012*
CA199	0.993 (0.987-0.999)	0.057		

*$p < 0.05$.

HCC – hepatocellular carcinoma, OR – odds ratio, CI – confidence interval, BMI – body mass index, CA153 – cancer antigen 153, ALT – alanine aminotransferase, AST – aspartate aminotransferase, AFP – alpha-fetoprotein, CEA – carcinoembryonic antigen, MVI – microvascular invasion
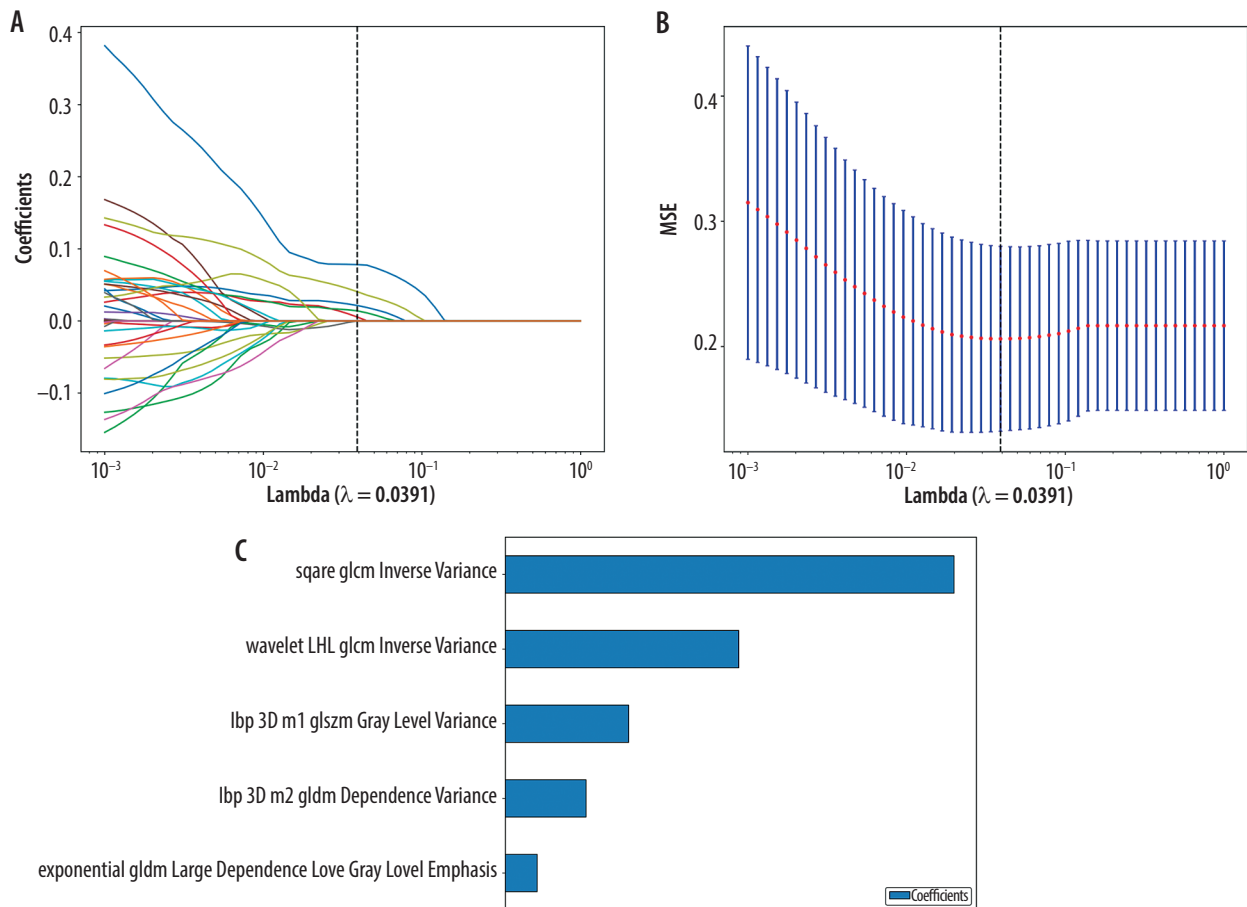

Figure 3. LASSO regression analysis results. **A**) Feature coefficient paths with optimal lambda value ($\lambda = 0.0391$). **B**) Mean squared error curve from 10-fold cross-validation. **C**) Coefficient values of the selected radiomic features.

LASSO – least absolute shrinkage and selection operator, MSE – mean squared error, GLDM – grey level dependence matrix, GLCM – grey level co-occurrence matrix
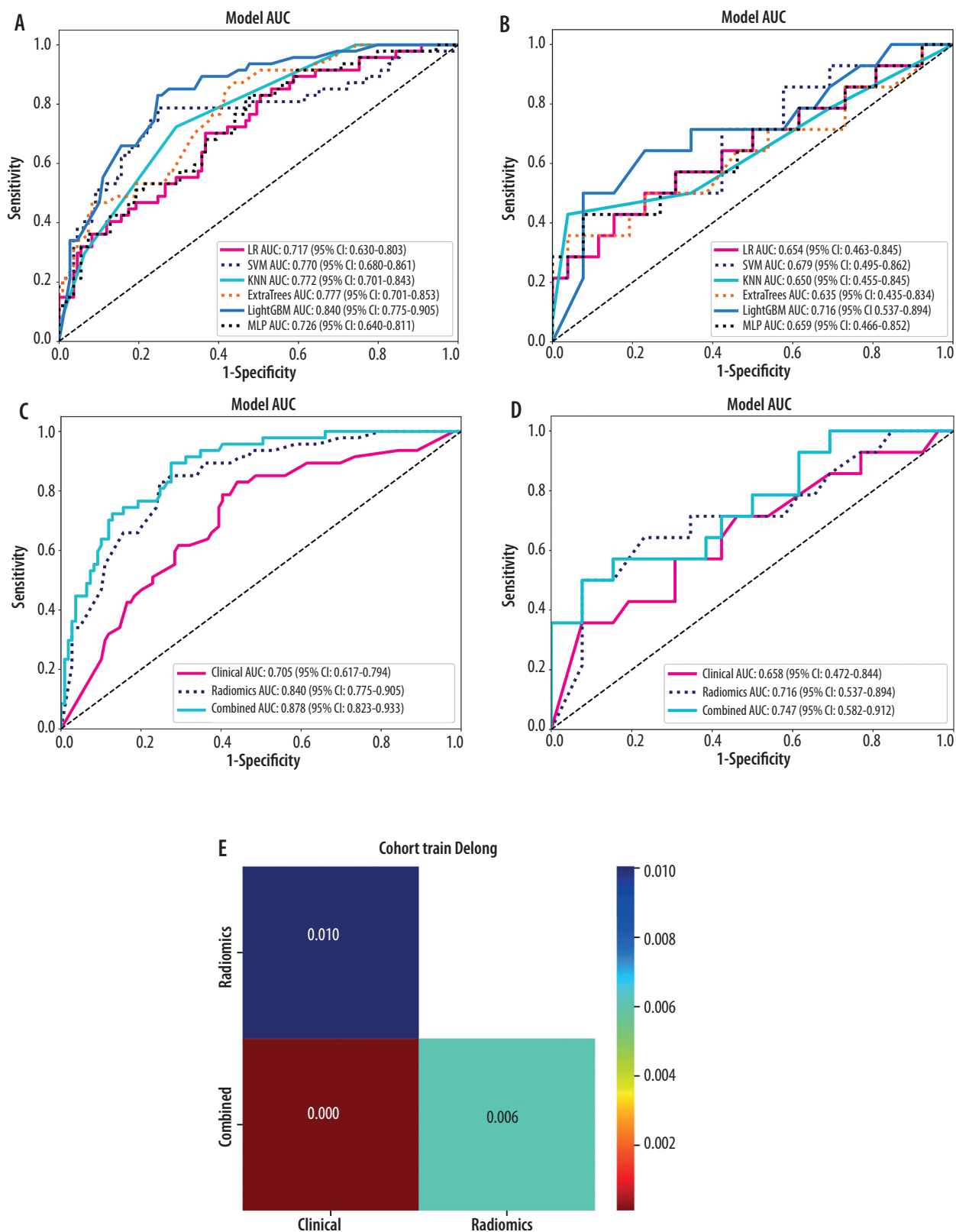
Figure 4. Comparison of model performance in predicting HCC pathological differentiation. **A**) ROC curves comparing 6 machine learning algorithms in the training cohort, showing LightGBM achieved the highest AUC (0.840). **B**) ROC curves of the algorithms in the testing cohort, with LightGBM maintaining superior performance (AUC = 0.716). **C**) ROC curves comparing the clinical model (AUC = 0.705), radiomics model (AUC = 0.840), and combined model (AUC = 0.878) in the training cohort. **D**) Model comparison in the testing cohort, demonstrating maintained performance of the combined model (AUC = 0.747). **E**) Heat map of DeLong test results showing significant differences between the combined model and individual models ($p < 0.05$)

ROC – receiver operating characteristic, AUC – area under the curve, CI – confidence interval, LightGBM – light gradient boosting machine, HCC – hepatocellular carcinoma

and radiomics features, the LightGBM algorithm was selected as the basis for the radiomics component.

Model performance evaluation

The clinical model showed an AUC of 0.705 (95% CI: 0.617-0.794) in the training cohort and 0.658 (95% CI: 0.472-0.844) in the testing cohort. The radiomics model based on LightGBM demonstrated improved performance with AUCs of 0.840 (95% CI: 0.775-0.905) and 0.716 (95% CI: 0.537-0.894) in the respective cohorts. The combined model, integrating both clinical and radiomic features, achieved the highest diagnostic performance with AUCs of 0.878 (95% CI: 0.823-0.933) in the training cohort and 0.747 (95% CI: 0.582-0.918) in the testing cohort (Figure 4C and D). Statistical comparison

using DeLong tests revealed significant differences between the combined model and both the clinical and radiomics models in the training cohort ($p < 0.05$) (Figure 4E). These results suggest that the combined model provides superior discriminative ability for predicting HCC pathological differentiation compared to either the clinical or radiomics model alone.

Clinical utility assessment

The calibration curves demonstrated good agreement between predicted and observed probabilities for the combined model in both cohorts (Figure 5A). Among the 3 curves shown, the combined model exhibited better calibration than either the clinical or radiomics model alone, suggesting reliable prediction performance.
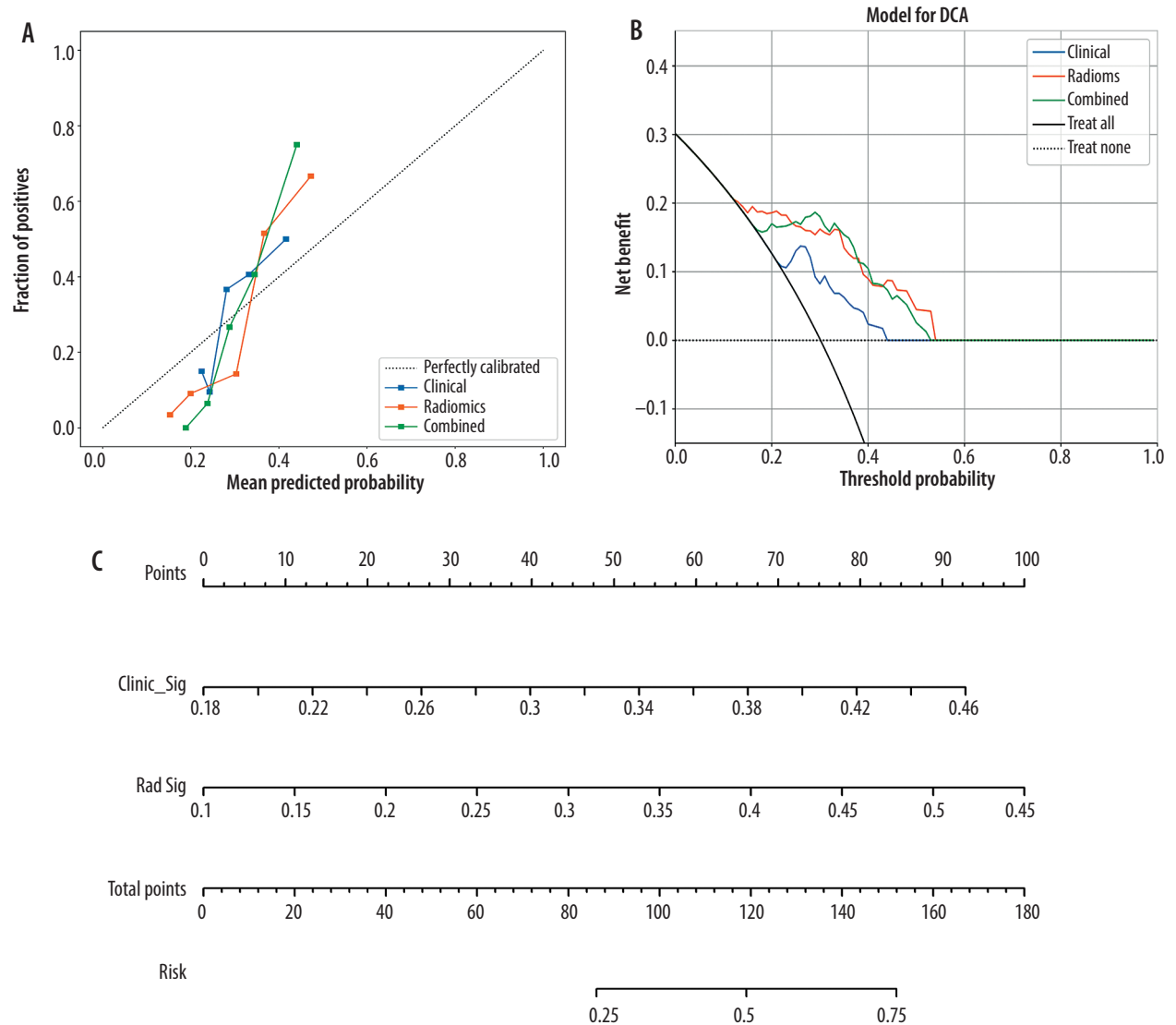

Figure 5. Performance evaluation and nomogram drawing of prediction models for pathological differentiation degree. **A**) Calibration curves comparing the agreement between predicted and observed probabilities in the training cohort for clinical, radiomics, and combined models. **B**) Decision curve analysis showing the net benefit of different models across various threshold probabilities. **C**) Nomogram integrating clinical and radiomics signatures for individualised prediction of hepatocellular carcinoma differentiation risk

Decision curve analysis was performed to evaluate the clinical utility of different prediction models (Figure 5B). The net benefit was calculated by subtracting the proportion of false-positive results from true-positive results, weighted by the relative harm of unnecessary treatment versus missed treatment. The analysis showed that the combined model (green line) provided consistently higher net benefit compared to both the clinical model (blue line) and radiomics model (orange line) across a wide range of threshold probabilities (0.2-0.6). This indicates that the combined model would be more clinically useful than treating all patients as poorly differentiated (grey line) or non-poorly differentiated (black line).

To facilitate clinical application, a nomogram was constructed incorporating both clinical signature (Clinic_Sig) and radiomics signature (Rad_Sig) (Figure 5C). For individual patients, points are assigned for each signature based on their values (ranging from 0.18 to 0.46 for clinical signature and 0.1 to 0.55 for radiomics signature). The total points (0-180) can be converted to a corresponding risk probability (0.25-0.75) of poor differentiation. This visual tool provides clinicians with an intuitive method to estimate an individual patient's risk of poor differentiation.

Discussion

This study developed and validated a novel combined model integrating CT radiomics features with clinical parameters for predicting HCC pathological differentiation. Our findings demonstrated superior predictive performance of the combined approach compared to individual clinical or radiomics models. The developed nomogram provides an intuitive tool for clinical implementation.

Our analysis revealed significant associations between BMI, CA153, and HCC differentiation. Elevated BMI has been previously identified as a risk factor for aggressive cancer subtypes, particularly in premenopausal breast cancer patients who show increased susceptibility to triple-negative and non-luminal subtypes [23,24]. The underlying mechanism may involve specific molecular pathways and adipokine interactions that enhance tumour aggressiveness in individuals with higher BMI [25]. Similarly, CA153, traditionally employed in breast cancer diagnosis with 63% sensitivity and 82% specificity [26], emerged as a significant predictor in our study. This finding aligns with established correlations between poor differentiation and increased tumour aggressiveness [5].

The clinical model, incorporating only BMI and CA153, demonstrated moderate predictive capability with AUCs of 0.705 (95% CI: 0.339-0.545) and 0.658 (95% CI: 0.353-0.685) in the training and testing cohorts, respectively. These results suggest potential limitations of clinical parameters alone in characterising HCC biological features [27]. Further investigation of the molecular mechanisms underlying these associations through *in vivo* and *in vitro* studies may provide additional insights into HCC development and progression.

Radiomics represents an emerging field in medical imaging analysis that extracts quantitative features through mathematical algorithms to enhance diagnostic accuracy. The integration of machine learning (ML) algorithms with radiomics features enables the development of predictive models capable of capturing tumour heterogeneity at the microscopic level [21,28]. In our study, we initially extracted 1834 radiomics features from CT images, encompassing various categories such as first-order statistics, shape-based features, and texture parameters. Through careful dimensionality reduction, 5 key features were ultimately selected for model construction.

To ensure robust model development, we evaluated 6 different ML classifiers for predicting HCC pathological differentiation. The LightGBM algorithm emerged as the optimal classifier, demonstrating superior performance with AUCs of 0.840 (95% CI: 0.775-0.905) and 0.716 (95% CI: 0.537-0.894) in the training and testing cohorts, respectively. These results present interesting contrasts with previous research. For instance, Chen *et al.* [29] reported optimal performance using SVM classifiers with portal venous phase images, while Hu *et al.* [30] achieved better results using LR classifiers, with AUCs of 0.75 and 0.70 for training and testing cohorts, respectively. The variation in classifier performance across studies can be attributed to several technical factors, including differences in CT scanning parameters (such as slice thickness and contrast enhancement timing) and reconstruction algorithms [31].

Our comprehensive analysis revealed that classifier performance is inherently dependent on the specific characteristics of the input data, suggesting that no single classifier universally outperforms others. This observation supports our strategy of implementing multiple classifiers for model development because it allows for optimal algorithm selection based on specific dataset characteristics. The successful integration of extensive radiomic features with multiple ML classifiers in our study not only improved the accuracy of HCC differentiation prediction but also demonstrated the potential of radiomics as an advanced diagnostic tool. This approach provides valuable insights into the development of more accurate and robust predictive models in radiomics research.

Finally, the combined clinical-radiomics model, integrating BMI, CA153, and radiomic features, demonstrated superior predictive performance compared to individual models, achieving AUCs of 0.878 (95% CI: 0.823-0.933) and 0.747 (95% CI: 0.582-0.912) in the training and testing cohorts, respectively. Different from the research of Li *et al.* [20] and Liu *et al.* [32], we integrate clinical and radiomics, which can improve the prediction performance of the model, better reflect the reliability of radiomics technology, and at the same time promote the development of machine learning.

Applications in medicine. We then drew this combined model into a visual nomogram, which can more intuitively display the relationship between clinical features and radiomics feature scores and HCC pathological differentiation. DCA of the combined model showed that for HCC patients with predicted pathological differentiation, the combined model provided the best benefit within a given threshold probability range with better clinical benefit. The potential to accurately predict pathological differentiation before surgery and improve individualised clinical diagnosis of HCC differentiation is of great significance to assist clinicians in formulating more accurate treatment plans in a timely manner.

Our study has several limitations that should be addressed in future studies: 1) The single-centre retrospective design and small sample size may introduce selection bias. Future studies should include multicentre data to validate and expand the generalisability of the results. 2) Manual delineation of original lesion boundaries may not completely avoid errors in poorly defined tumours. Advanced segmentation algorithms could improve this aspect in future research. 3) Our study only analysed the poorly differentiated group and the non-poorly differentiated group, and subsequent experiments hope to find better methods to predict the pathological differentiation of high, medium, and low hepatocellular carcinoma. To address these limitations and further validate our findings, we are planning a prospective, multicentre study that will include more HCC patients, incorporate more radiomics features, and add an external validation model.

Conclusions

This study demonstrates that a machine learning-based CT radiomics model combining clinical and imaging features can effectively predict HCC pathological differentiation. The model's non-invasive nature and promising predictive performance show its potential value as a preoperative assessment tool. The developed nomogram provides clinicians with an intuitive method for estimating differentiation risk, which could facilitate treatment planning and potentially improve patient outcomes.

Disclosures

References

1. Mao XC, Shi S, Yan LJ, Wang HC, Ding ZN, Liu H, et al. A model based on adipose and muscle-related indicators evaluated by CT images for predicting microvascular invasion in HCC patients. Biomark Res 2023; 11: 87. DOI: https://doi.org/10.1186/s40364-023-00527-z.

2. Jiang C, Cai YQ, Yang JJ, Ma CY, Chen JX, Huang L, et al. Radiomics in the diagnosis and treatment of hepatocellular carcinoma. Hepatobiliary Pancreat Dis Int 2023; 22: 346-351.

3. Greten TF, Villanueva A, Korangy F, Ruf B, Yarchoan M, Ma L, et al. Biomarkers for immunotherapy of hepatocellular carcinoma. Nat Rev Clin Oncol 2023; 20: 780-798.

4. Ozer Etik D, Suna N, Boyacioglu AS. Management of hepatocellular carcinoma: prevention, surveillance, diagnosis, and staging. Exp Clin Transplant 2017; 15: 31-35.

5. Martins-Filho SN, Paiva C, Azevedo RS, Alves VAF. Histological grading of hepatocellular carcinoma – a systematic review of literature. Front Med (Lausanne) 2017; 4: 193. DOI: https://doi.org/10.3389/fmed.2017.00193.

6. Sasaki K, Matsuda M, Ohkura Y, Kawamura Y, Inoue M, Hashimoto M, et al. In hepatocellular carcinomas, any proportion of poorly differentiated components is associated with poor prognosis after hepatectomy. World J Surg 2014; 38: 1147-1153.

7. Wang L, Wang J, Zhang X, Li J, Wei X, Cheng J, et al. Diagnostic value of preoperative needle biopsy for tumor grading assessment in hepatocellular carcinoma. PLoS One 2015; 10: e0144216. DOI: https://doi.org/10.1371/journal.pone.0144216.

8. Kleiner DE. Hepatocellular carcinoma: liver biopsy in the balance. Hepatology 2018; 68: 13-15.

9. Zhang K, Li WC, Xie SS, Lin LY, Shen ZW, Ye ZX, Shen W. Preoperative determination of pathological grades of primary single HCC: development and validation of a scoring model. Abdom Radiol (NY) 2022; 47: 3468-3477.

10. An C, Park MS, Jeon HM, Kim YE, Chung WS, Chung YE, et al. Prediction of the histopathological grade of hepatocellular carcinoma using qualitative diffusion-weighted, dynamic, and hepatobiliary phase MRI. Eur Radiol 2012; 22: 1701-1708.

11. Qian H, Shen Z, Zhou D, Huang Y. Intratumoral and peritumoral radiomics model based on abdominal ultrasound for predicting Ki-67 expression in patients with hepatocellular cancer. Front Oncol 2023; 13: 1209111. DOI: https://doi.org/10.3389/fonc.2023.1209111.

12. Qin X, Hu X, Xiao W, Zhu C, Ma Q, Zhang C. Preoperative evaluation of hepatocellular carcinoma differentiation using contrast-enhanced ultrasound-based deep-learning radiomics model. J Hepatocell Carcinoma 2023; 10: 157-168.

13. Bi WL, Hosny A, Schabath MB, Giger ML, Birkbak NJ, Mehrtash A, et al. Artificial intelligence in cancer imaging: clinical challenges and applications. CA Cancer J Clin 2019; 69: 127-157.

14. Lambin P, Leijenaar RTH, Deist TM, Peerlings J, de Jong EEC, van Timmeren J, et al. Radiomics: the bridge between medical imaging and personalized medicine. Nat Rev Clin Oncol 2017; 14: 749-762.

15. Miranda Magalhaes Santos JM, Clemente Oliveira B, Araujo-Filho JAB, Assuncao-Jr AN, de M Machado FA, Carlos Tavares Rocha C, et al. State-of-the-art in radiomics of hepatocellular carcinoma: a review of basic principles, applications, and limitations. Abdom Radiol (NY) 2020; 45: 342-353.

16. Cao K, Wang X, Xu C, Wu L, Li L, Yuan Y, Ye X, et al. Ultrasound-based radiomics analysis for assessing risk factors associated with early recurrence following surgical resection of hepatocellular carcinoma. Ultrasound Med Biol 2024; 50: 1964-1972.

17. Yang C, Zhang ZM, Zhao ZP, Wang ZQ, Zheng J, Xiao HJ, et al. Radiomic analysis based on magnetic resonance imaging for the prediction of VEGF expression in hepatocellular carcinoma patients. Abdom Radiol (NY) 2024; 49: 3824-3833.

18. Kuang F, Gao Y, Zhou Q, Lu C, Lin Q, Al Mamun A, et al. MRI radiomics combined with clinicopathological factors for predicting 3-year overall survival of hepatocellular carcinoma after hepatectomy. J Hepatocell Carcinoma 2024; 11: 1445-1457.

19. Huang Y, Chen L, Ding Q, Zhang H, Zhong Y, Zhang X, Weng S. CT-based radiomics for predicting pathological grade in hepatocellular carcinoma. Front Oncol 2024; 14: 1295575. DOI: https://doi.org/10.3389/fonc.2024.1295575.

20. Li C, Xu J, Liu Y, Wu M, Dai W, Song J, Wang H. Kupffer phase radiomics signature in sonazoid-enhanced ultrasound is an independent and effective predictor of the pathologic grade of hepatocellular carcinoma. J Oncol 2022; 2022: 6123242. DOI: https://doi.org/10.1155/2022/6123242.

21. Liu HF, Lu Y, Wang Q, Lu YJ, Xing W. Machine learning-based CEMRI radiomics integrating LI-RADS features achieves optimal evaluation of hepatocellular carcinoma differentiation. J Hepatocell Carcinoma 2023; 10: 2103-2115.

22. Nagtegaal ID, Odze RD, Klimstra D, Paradis V, Rugge M, Schirmacher P, et al. The 2019 WHO classification of tumours of the digestive system. Histopathology 2020; 76: 182-188.

23. Kwan ML, Kroenke CH, Sweeney C, Bernard PS, Weltzien EK, Castillo A, et al. Association of high obesity with PAM50 breast cancer intrinsic subtypes and gene expression. BMC Cancer 2015; 15: 278. DOI: https://doi.org/10.1186/s12885-015-1263-4.

24. Torres-de la Roche LA, Steljes I, Janni W, Friedl TWP, De Wilde RL. The association between obesity and premenopausal breast cancer according to intrinsic subtypes – a systematic review. Geburtshilfe Frauenheilkd 2020; 80: 601-610.

25. Di Filippo G, Canu GL, Lazzari G, Serbusca D, Morelli E, Brazzarola P, et al. Exploring the link between BMI and aggressive histopathological subtypes in differentiated thyroid carcinoma-insights from a multicentre retrospective study. Cancers (Basel) 2024; 16: 1429. DOI: https://doi.org/10.3390/cancers16071429.

26. Tang S, Wei L, Sun Y, Zhou F, Zhu S, Yang R, et al. CA153 in breast secretions as a potential molecular marker for diagnosing breast cancer: a meta analysis. PLoS One 2016; 11: e0163030. DOI: https://doi.org/10.1371/journal.pone.0163030.

27. Lv K, Cao X, Du P, Fu JY, Geng DY, Zhang J. Radiomics for the detection of microvascular invasion in hepatocellular carcinoma. World J Gastroenterol 2022; 28: 2176-2183.

28. Gillies RJ, Kinahan PE, Hricak H. Radiomics: images are more than pictures, they are data. Radiology 2016; 278: 563-577.

29. Chen W, Zhang T, Xu L, Zhao L, Liu H, Gu LR, et al. Radiomics analysis of contrast-enhanced CT for hepatocellular carcinoma grading. Front Oncol 2021; 11: 660509. DOI: https://doi.org/10.3389/fonc.2021.660509.

30. Hu X, Li C, Wang Q, Wu X, Chen Z, Xia F, et al. Development and external validation of a radiomics model derived from preoperative gadoxetic acid-enhanced MRI for predicting histopathologic grade of hepatocellular carcinoma. Diagnostics (Basel) 2023; 13: 413. DOI: https://doi.org/10.3390/diagnostics13030413.

31. Wang Q, Li C, Zhang J, Hu X, Fan Y, Ma K, et al. Radiomics models for predicting microvascular invasion in hepatocellular carcinoma: a systematic review and radiomics quality score assessment. Cancers (Basel) 2021; 13: 5864. DOI: https://doi.org/10.3390/cancers13225864.

32. Liu HF, Wang M, Wang Q, Lu Y, Lu YJ, Sheng Y, et al. Multiparametric MRI-based intratumoral and peritumoral radiomics for predicting the pathological differentiation of hepatocellular carcinoma. Insights Imaging 2024; 15: 97. DOI: https://doi.org/10.1186/s13244-024-01623-w.